Comparative performance and eco-toxicity assessment of $Y_2(CO_3)_3$), ZnO/TiO_2, and Fe_3O_4 nanoparticles for arsenic removal from water

H. Salazar[1,2], P. M. Martins[3,4,†], Daniela Batista[3,4], K. P. Shejale[5], R. K. Sharma[5], Krishnapriya R.[5], S. Ferdov[1], G. Botelho[2], A. Fidalgo-Marijuan[6], Fernanda Cássio[3,4] and S. Lanceros-Mendez[6,7,†]

[1]Centre/Department of Physics, [2]Centre/Department of Chemistry, [3]Centre of Molecular and Environmental Biology, University of Minho, Campus de Gualtar, 4710-057 Braga, Portugal

[4]IB-S – Institute for Research and Innovation on Bio-Sustainability, University of Minho, 4710-057, Braga, Portugal

[5]Department of Chemistry, Indian Institute of Technology of Jodhpur

[6]BCMaterials, Basque Center for Materials, Applications and Nanostructures, UPV/EHU Science Park, 48940 Leioa, Spain

[7]IKERBASQUE, Basque Foundation for Science, 48009 Bilbao, Spain

† Corresponding authors: pamartins@fisica.uminho.pt

Abstract

The application of nanomaterials to remove arsenic (As) from the water represents one of the most promising remediation methods nowadays. In this study, three active materials, including $Y_2(CO_3)_3$), ZnO/TiO_2, and Fe_3O_4, with different structural and morphological properties, were evaluated for their As(V) adsorption capacity in contaminated water. Thus, the adsorption behaviour was evaluated, including the influence of pH, absorption kinetics, and isotherms. This work demonstrates that the active materials show a high adsorption performance, with adsorption efficiencies always close to 100%, leading to maximum adsorption capacities of 32.8, 37.3, and 35.8 mg/g for $Y_2(CO_3)_3$), ZnO/TiO_2, and Fe_3O_4, respectively. The effects of these suspended sorbent nanomaterials on *Daphnia magna* allowed us to estimate the lethal concentration that kills 50% of the test specimens (LC_{50}) of $6.57x10^3$ mg/L, 28.7 mg/L, and

$1.91x10^6$ mg/L, for Fe_3O_4, ZnO/TiO_2 and $Y_2(CO_3)_3$, respectively. Overall, it is confirmed the suitability of the investigated materials for arsenic water remediation applications.

Keywords: adsorption, arsenic, ecotoxicity, heavy-metals, nanomaterials, water remediation

1. Introduction

Water quality is a growing concern throughout the world, and the problems caused by the scarcity of potable water imply that 1.2 billion people do not have access to drinkable water. Additionally, 2.6 billion people have little or no sanitation, and approximately 4000 children die every day due to diseases caused by bacteria and viruses transmitted through contaminated water [1].

Arsenic (As) is a ubiquitous element naturally found in the lithosphere (soil, rocks and water) and is one of the twenty most abundant elements in the environment [2]. It is present in the atmosphere, hydrosphere and biosphere in different concentrations and as compound or elemental [3]. It is unusual to find arsenic in elemental form; it is typically conjugated with oxygen, sulphur, and iron. The arsenic compounds most commonly present in nature are arsenite (+3) and arsenate (+5) [4]. The predominance of each form depends on the environment to which they are exposed. Arsenate is generally the most stable state in oxidative environments, while in reductive environments, it is reduced to its most toxic form: As (III). These ionised forms are the reference for the technologies for removing arsenic from water [5].

Arsenic is present in water due to both natural and anthropogenic causes [3]. Naturally arsenic occurrence is due to the weathering and dissociation of rocks or minerals that contain arsenic. Anthropogenically, arsenic occurs mainly due to mining activity and industry. The natural concentration of As in the soils is typically between 5 and 10 mg/kg, while in groundwater ranges from 0.5 to 5000 μg/L [6]. Arsenic is one of the most potential carcinogens, and it presents a complicated metabolism when compared with the "big four" toxic non-essential elements (As, cadmium (Cd), mercury (Hg) and lead (Pb)), being classified as Group

I human carcinogen by the World Health Organization (WHO) [7]. Long term arsenic exposure, which can occur through water, air, and soil, causes skin lesions, cancer, cardiovascular diseases, pulmonary problems, neurological deficiencies, and developmental and reproductive toxicity [8-10]. As a result, the WHO has set its maximum concentration level (MCL) in drinking water to 10 µg/L [6]. Water exposure is the most critical way arsenic gets into the human body since most of the compounds are easily dissolved in water. In this context, the United Nations International Children Emergency Fund (UNICEF) has been developing efforts with governments in countries where this chemical is a severe problem, such as Bangladesh, India, China and Vietnam, promoting the adoption of filtration technologies to treat contaminated water [10].

Different techniques for As removal from groundwater have been proposed, including oxidation [11], coagulation-flocculation [12], ion-exchange [13], membrane [10] and adsorption [14]. Among these, adsorption is one of the most promising techniques for removing inorganic pollutants, such as arsenic, due to its consistent efficiency, cost-effectiveness and simple operation [15]. Adsorption is a physicochemical process where solid or liquids surfaces retain dissolved substances. It can be classified into physical adsorption or van der Waal's adsorption and chemical adsorption or chemisorption [16]. Usually, gases and dissolved substances are adsorbed on a surface by weak van der Waal's adsorption, essentially depending on the surface area of the adsorbent at a given temperature and pressure. In the case of arsenic adsorption, the primary mechanism is the bound of the arsenic species to the surface of the adsorbent with the help of van der Waal's forces, which is separated from the solution by filtration or another separation process. This process depends on different factors, such as arsenic concentration, pH of the solution, temperature, and presence of other ionic species in the solution. The size of the adsorbents is usually in the nanometre range and with large porosity, providing a large surface area. There are a large variety of adsorbents with potential

efficiency in arsenic removal from water. These include activated carbon [17], activated alumina [18], fly ash [19], red mud [20], rice husk [21], kaolinite [22], goethite [23], chitosan [24] and cation-exchange resins [25]. Micro/nanomaterials as iron and aluminium oxides [26, 27], zinc oxide [28], yttrium [29], zeolites [30], clinoptilolite [31] and titanium dioxide-based materials [32] are being investigated for arsenic removal from water due to their high affinity towards inorganic species of arsenic and their high specific surface area.

In this work, the As(V) adsorption efficiency of nano/microparticles of yttrium carbonate ($Y_2(CO_3)_3$), zinc oxide/titanium dioxide (ZnO/TiO_2), and magnetite (Fe_3O_4), with different structural and morphological properties, was evaluated. The selection of the adsorbent materials has been carried out considering that yttrium-based adsorbents have been reported as materials with As adsorption capacity in all ranges of pH [33]. In addition, TiO_2-based materials also have been reported for As remediation due to their stability, high affinity for arsenic, and ability to oxidise As(III) and organic arsenic to As(V) [34], and that iron oxides are a well-known adsorbent for arsenic due to their high affinity for arsenic oxyanions and low cost [35]. The characterisation of the materials was performed and related to the As(V) adsorption efficiency under different experimental conditions such as pH, time of contact and arsenic concentrations. In addition, the potential toxicity of materials was examined using the model organism *Daphnia magna* and standard toxicity tests.

2. Materials and methods

2.1. Materials and reagents

Yttrium (III) carbonate, ($Y_2(CO_3)_3$, 99.9%, 100–120 nm, 35–65 m^2/g) was purchased from Sigma-Aldrich. 10 wt. % ZnO/TiO_2 nanoparticles were synthesised following the procedure reported in [36]. Magnetite nanoparticles (Fe_3O_4, 97.0%, 50–100 nm, 6–8 m^2/g) were obtained from Nanostructured & Amorphous Materials, Inc. Arsenic standard solution (H_3AsO_4, 1000

105 mg/L) was supplied by Merck. Sodium hydroxide (NaOH, ≥ 95%) and hydrochloric acid (HCl
106 37%) were acquired from Panreac and Sigma-Aldrich.
107
108 **2.2. Materials characterisation**
109 The crystalline structure of the micro/nanomaterials was characterised by X-ray diffraction
110 (XRD), using a Philips Analytical X-Ray PW1710 BASED diffractometer with Cu K_α
111 radiation, λ = 1.5406 Å (40 kV, 30 mA), over the scanning range 2θ = 10-80° with a step width
112 of 2°/min.
113 Transmission Electron Microscopy (TEM) was performed with a TECNAI G2 20 TWIN
114 apparatus operated at 200 kV and equipped with LaB_6 filament, EDAX EDS microanalysis
115 system and high angle annular dark-field-scanning transmission electron microscopy (HAADF-
116 STEM). The samples for the TEM experiments were prepared by dispersion into ethanol and
117 keeping the suspension in an ultrasonic bath for 15 min. Then, a drop of the suspension was
118 poured onto a TEM copper grid (300 mesh) covered by a pure carbon film and dried under
119 vacuum.
120 The zeta (ζ) potential was measured using a Zetasizer NANO ZS-ZEN3600, Malvern
121 (Malvern Instruments Limited, UK), equipped with a He–Ne laser (wavelength 633 nm) and
122 backscatter detection (173°). Nanoparticles were dispersed in ultra-pure water, and the solutions
123 were prepared at different pH values (3, 5, 7, 9 and 11) using HCl (1M) and NaOH (1M)
124 solutions. The results were obtained using the Smoluchowski theory approximation, and each
125 sample was measured ten times at 22 °C. The manufacturer software (Zetasizer 7.12) was used
126 to assess zeta potential values.
127 The specific surface area of the micro/nanomaterials was determined by the Brunauer-
128 Emmett-Teller (BET) method. The samples were analysed at -176 °C by nitrogen adsorption-

desorption in a Micromeritics TriStar analyser (Micromeritics). Before adsorption experiments, 0.5 g of each sample was outgassed at 26.7 Pa and 350 °C for six hours.

2.3. Arsenic removal efficiency evaluation

To evaluate the arsenic (As) removal efficiency of the materials, As(V) solutions were prepared by diluting a commercial standard solution of 1000 mg/L in ultrapure water.

Then, 50 mg of each adsorbent material was added to 50 mL of an As(V) standard solution. The solution was placed under magnetic stirring for 30 minutes and filtered to remove the materials from the solution. Three micro/nanomaterials were tested to evaluate their arsenic adsorption efficiency: $Y_2(CO_3)_3$, ZnO/TiO_2, and Fe_3O_4. Atomic absorption spectroscopy (AAS) was used to quantify the final As concentration in solutions and, therefore, to determine the adsorption capacity of the materials. The measurements were performed in a Thermo M Series AA Spectrometer coupled to a graphite furnace Thermo GF95Z Zeeman Furnace in a coated cuvette with defined conditions: λ = 193.7 nm; drying temperature = 100 °C; pyrolysis temperature = 1200 °C; atomising temperature = 2600 °C; cleaning temperature = 2800 °C.

Arsenic adsorption efficiency (E) and arsenic adsorption capacity (Q_e) were evaluated according to equations 1 and 2:

$$E\ (\%) = \frac{(C_i - C_f)}{C_i} \times 100 \quad (1)$$

$$Q_e = \frac{(C_i - C_f)V}{m} \quad (2)$$

where C_f and C_i are the final and initial arsenic concentration (mg/L), respectively, m is the mass (g) of adsorbent, and V is the volume (L) of the solution.

Experiments were performed under varying conditions, including different pH (2, 4, 7, and 10), contact times (2, 4, 6, 8, 10, 15, 20, 25, and 30 minutes), and As(V) initial concentrations (0.1, 0.25, 0.5, 0.75, 1, 2, 5, and 10 mg/L).

154 The kinetic behaviour was fitted according to non-linear forms of pseudo-first-order [37],
155 pseudo-second-order [38], Elovich [39], and Bangham models [40] described in Supplementary
156 Information. The isotherm curves were fitted according to non-linear forms of Langmuir [41],
157 Freundlich [42], Temkin [43], and Dubinin-Radushkevich [44] models, described in
158 Supplementary Information.
159
160 **2.4. Acute lethality tests**
161 Acute lethality tests were performed to evaluate the sensitivity of the *Daphnia magna* to the
162 different nanoparticles (Fe_3O_4, ZnO/TiO_2 and $Y2(CO_3)_3$). Individuals of *D. magna* were placed
163 in containers with 10 mL of nanosuspensions (n=5). For each concentration, four replicates
164 were used. Subsequently, they were exposed to the nanoparticle's suspensions prepared in
165 autoclaved mineral water (6 concentrations ranging from 0 to 2000 mg/L of Fe_3O_4; 0.1 to 50
166 mg/L of ZnO/TiO_2; and 0.005 to 1.5 mg/L of $Y_2(CO_3)_3$). The tests ran for 48 h at 21 ºC under
167 a 12 h:12 h photoperiod. The animals were not fed during exposure. Individuals that did not
168 show any movement when mechanically stimulated at 24 h intervals were considered dead. At
169 the beginning and after 48 h, the pH of the nanosuspensions was measured (Table S1). *Daphnia*
170 *magna* mortality recorded in the acute toxicity tests was used to calculate the mean
171 concentration and 95% of confidence interval (C. I.), inducing the death of 50% of the test
172 specimens (LC_{50}) within 48 h of exposure. PriProbit 1.63 [45] was used to estimate toxicity
173 parameters. Repeated measurements analysis of variance (ANOVA) was used to test for effects
174 of nanoparticles concentrations on the percentage of animal survival in the acute lethality test
175 [46].
176
177 # 3. Results and discussion
178 **3.1. Nanomaterial's characterisation**

Materials characterisation was carried out through TEM, XRD, BET surface area and zeta potential measurements. Figure 1 (a, b, c) shows representative TEM images of Fe3O4, ZnO/TiO_2 and $Y_2(CO_3)_3$. TEM images of Fe_3O_4 show spherical and hexagonal particles, with diameters ranging from 80 to 150 nm. For ZnO/TiO_2 nanoparticles, round-shaped particles are observed, presenting widths from 100 to 350 nm. $Y_2(CO_3)_3$ nanoparticles exhibit a shape like nanorods with varying sizes and lengths ranging from 50 to 200 nm.

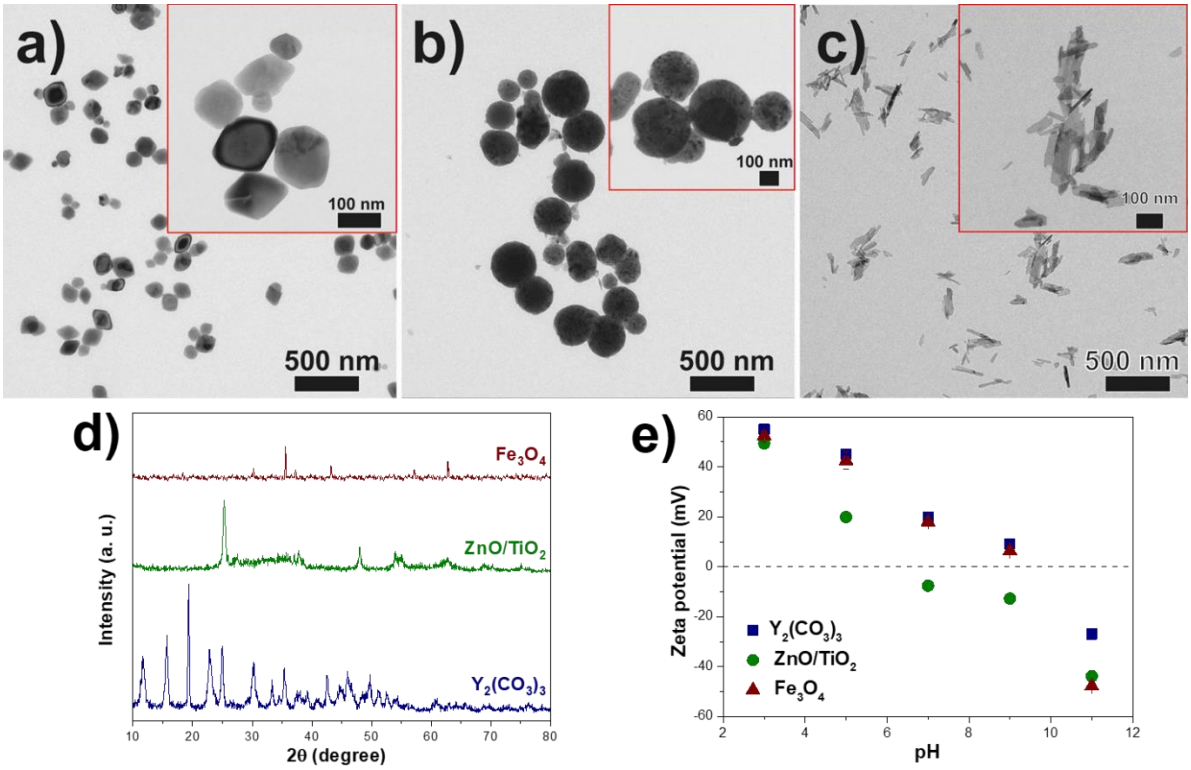

Figure 1. TEM images of **(a)** Fe_3O_4, **(b)** ZnO/TiO_2 and **(c)** $Y_2(CO_3)_3$; **(d)** XRD patterns and **(e)** zeta potential measurements of magnetite, 10% ZnO/TiO_2 and $Y_2(CO_3)_3$.

The characterisation of the different nano/micro materials performed by XRD is shown in Figure 1 (d). $Y_2(CO_3)_3$ diffractogram presents peaks at 11.6º, 15.7º, 19.4º, 22.8º, 25.0º, 30.1º and 35.5º, which are characteristic of its crystalline form and agree with Y-Tengerite ($Y_2(CO_3)_3 \cdot 2$-$3H_2O$) [47-49]. Magnetite shows peaks at 2θ = 33.0º, 35.6º, 40.7, 49.3 53.9º, 62.4º and 63.9º, characteristic of a rhombohedral crystalline structure [50, 51]. The ZnO/TiO_2 diffractogram

191 shows the characteristic peaks of TiO_2 at 2θ = 25.3º, 37.8º, 54.1º, 55.0º and 62.8º [52, 53] and
192 one characteristic peak of ZnO at 2θ = 48.1º [53, 54]. Just one peak of ZnO is present in the
193 ZnO/TiO_2 nanocomposite diffractogram, related to the low amount of ZnO.

194 The zeta potential measurements are paramount to estimate the surface charge of the
195 particles. Figure 1 (e) shows a similar surface charge dependency on the pH for $Y_2(CO_3)_3$,
196 ZnO/TiO_2, and Fe_3O_4. All the nanomaterials present positive zeta potential values at acidic pH
197 values. The point of zero charges (PZC) of ZnO/TiO_2 is approximately at pH 6 and,
198 consequently, at pH values higher than PZC this nanomaterial is negatively charged. $Y_2(CO_3)_3$
199 and Fe_3O_4 show the PZC at pH 10, and just in highly alkaline conditions, these materials are
200 negatively charged. The surface area of these three materials was determined using the BET
201 method. The surface area of ZnO/TiO_2 is 88.28 m^2/g, showing a very low microporosity (the
202 micropore area is 9.911 m^2/g). The total pore volume is 0.144 cm^3/g, and pore distribution of 2
203 to 6 nm is observed, which is related to the nanoparticle size distribution. Both Fe_3O_4 and
204 $Y_2(CO_3)_3$ show no microporosity and a surface area of 1 m^2/g. In related studies, surface area
205 values of 31 m^2/g have been obtained using iron oxide for water treatment [55]. Previous works
206 with similar crystalline structures of $Y_2(CO_3)_3$ have reported surface area values ranging from
207 0.1 to 10 m^2/g [56, 57]. The synthesis process and the crystalline arrangement leads to different
208 morphologies and surface areas. A higher surface area promotes more interaction between the
209 adsorbent and the arsenic species, and better efficiency is expected. To overcome the smaller
210 surface area, the affinity of functional groups of $Y_2(CO_3)_3$ and Fe_3O_4 must also play a relevant
211 role to achieve effective arsenic adsorption.
212

213 **3.2. Arsenic removal efficiency evaluation**

An initial evaluation of the active materials was performed to identify the best pH of the media that leads to better arsenic removal efficiencies. After that, the adsorption kinetics and isotherms were evaluated under the optimised conditions.

3.2.1. Effect of pH

Arsenic species exist as neutral and anionic forms in the pH range of 2-10 [58]. Also, pH is an essential parameter because the functional groups and surface charge of active materials are affected by the pH of the solution, as previously mentioned in section 3.1. [59]. It is thus necessary to understand the influence of initial pH values on adsorption efficiency. Therefore, the three active materials were subjected to different pH values: 2, 4, 7 and 10 (Figure 2).

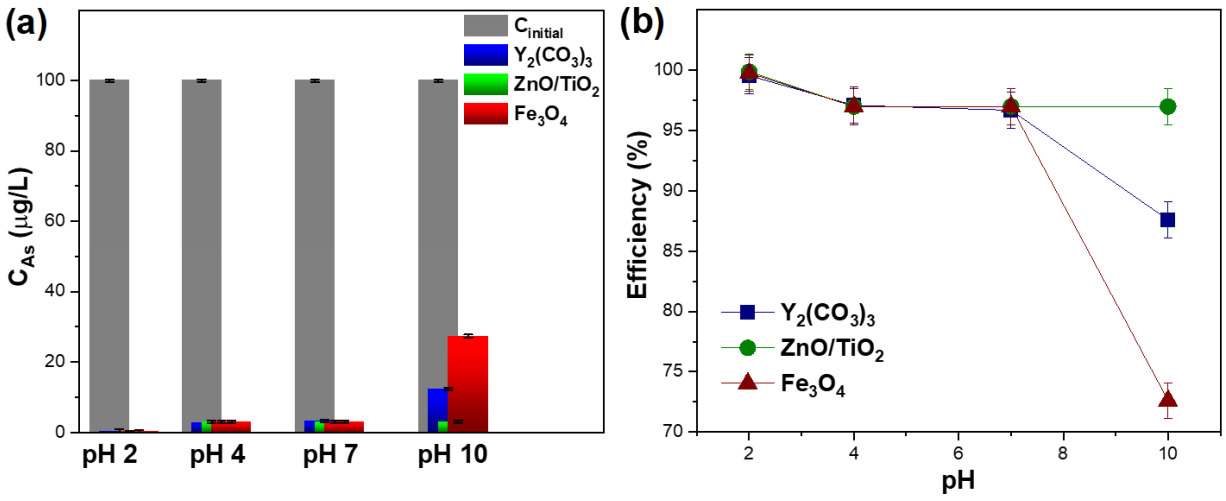

Figure 2. (a) Effect of pH on As(V) adsorption by $Y_2(CO_3)_3$, ZnO/TiO_2 and Fe_3O_4; **(b)** dependence of pH on the adsorption efficiency (contact time: 30 min; [As] = 100 µg/L; adsorbent dosage; 1 g/L).

Since the pH values affect the surface charges of the adsorbents and arsenic species, pH will directly affect the adsorption of As(V). As shown in Figure 2, for almost all materials, the As (V) adsorption capacity depends on pH, and the adsorption is significantly better under acidic and neutral environments. For pH 2, pH 4, and pH 7, all materials present adsorption efficiencies higher than 97%. Under alkaline conditions, at pH 10, the adsorption efficiency

decreases for almost all materials, except for ZnO/TiO_2. Thus, the performance of ZnO/TiO_2 is independent of the pH; contrarily, the adsorption efficiency of $Y_2(CO_3)_3$ and Fe_3O_4 depends on pH. The electrostatic repulsions between materials and As(V) species with increased pH explain this dependence. When pH < 7, the primary forms of As(V) in water are anions (AsO_4^{3-}, $HAsO_4^{2-}$ and $H_2AsO_4^-$), favouring the protonation of the adsorbent surface. The protons increase results in multiplying positively charged sites, leading to the enhanced attractive force between adsorbents and arsenic species [60]. Hence, at acidic pH values, there are many positive charges on the surface of the materials, promoting a strong attraction to the arsenic anions in the solution. However, the amount of OH^- increases with increasing pH, resulting in a competition for the As(V) adsorption on materials surface. When pH ≥ 10, positive charges appear on the surface of $Y_2(CO_3)_3$ and Fe_3O_4, and the adsorption capacity decreases. The independence of ZnO/TiO_2 from pH could be due to the larger surface area of this material, which allows better contact between arsenic species and the surface of the active material. These results evidence the role of electrostatic interaction, surface charge and surface area of the materials in the adsorption process.

3.2.2. Adsorption kinetics

The contact time is an essential parameter defining the adsorption efficiency. The effect of contact time between arsenic and the active materials was evaluated at contact times of 2, 4, 6, 8, 10, 15, 20, 25, and 30 minutes, as represented in Figure 3 (a).

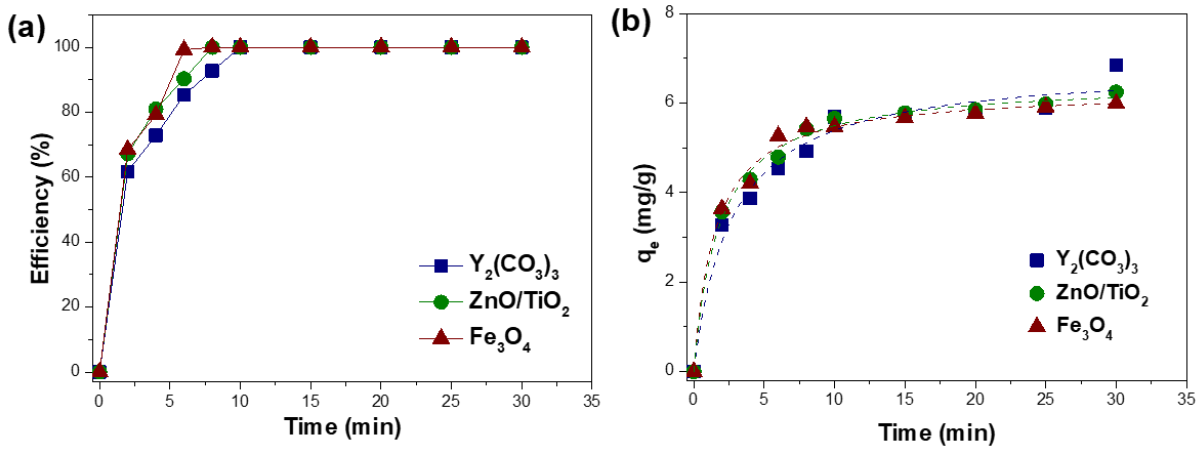

Figure 3. (a) Effect of contact time on arsenic adsorption by the active materials; **(b)** Pseudo-second order adsorption kinetics of $Y_2(CO_3)_3$, ZnO/TiO_2 and Fe_3O_4 (pH = 7; [As] = 100 µg/L; adsorbent dosage; 1 g/L).

Figure 3 (a) shows an initial high adsorption rate for all materials, as shown by the high adsorption efficiencies in the first 10 minutes of contact. For all materials, 100% of arsenic removal was achieved after the first 15 min. This faster adsorption occurs because, at the beginning of the process, a high number of active binding sites are available for adsorption and more As species are adsorbed. As the adsorption process continues, the active sites of the adsorbents begin to be unavailable. As a result, the adsorption rate slows down until it reaches equilibrium. This two-stage adsorption process has been described for arsenic adsorption [61, 62].

Adsorption kinetics is an important parameter to understand the behaviour of adsorption over time. Based on Figure 3 (a), most As(V) adsorption occurs in the first 10 minutes of contact with the active materials. With this data, As(V) adsorption kinetics was analysed using pseudo-first, pseudo-second-order, Elovich, and Bangham kinetic models. Figure 3 (b) presents the kinetics fitting using a pseudo-second-order model, whilst Figure S1 and Table S2 provide the adsorption kinetics fitting for all the simulated models. Table S1 also summarises the adsorption rate constants (k, α), the correlation coefficient (R^2), and the root-mean-square errors (RMSE) for each model.

Based on R^2 and RMSE values, the adsorption kinetics fits well with all the models. Among all, the pseudo-second-order model presents better R^2 and RMSE values for all active materials. As this model defines adsorption as a chemical process, it is reasonable to consider chemisorption as the main driving force for As(V) adsorption on active materials surfaces [63]. However, as R^2 and RMSE values of pseudo-second and pseudo-first-order models are similar, arsenic adsorption can be explained as a combination of electrostatic interactions (physical adsorption) and chemisorption [64, 65].

3.2.3. Adsorption isotherms

The adsorption capacity of the three active materials was evaluated through adsorption experiments using different As(V) concentrations, and the results are presented in Table S3. It was found that all active materials can remove As(V) completely, regardless of the initial concentration, as efficiencies higher than 97% are always obtained. The results show that all active materials remove As(V) to values below the MCL when the initial concentration is lower than 1 mg/L, which means that all materials are efficient to remove As in under concentrations that are typically found in arsenic polluted water sources around the world [66]. The fitting of As(V) adsorption isotherms using different models was performed with the obtained data. The fitting of Langmuir isotherm model to the experimental results is presented in Figure 4, whilst Figure S2 and Table S4 provide the adsorption isotherm fitting for all the simulated models.

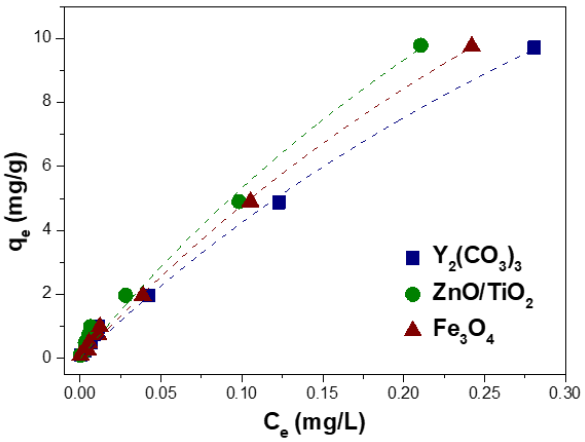

Figure 4. As(V) adsorption Langmuir isotherm of $Y_2(CO_3)_3$, ZnO/TiO_2 and Fe_3O_4 (pH = 7; contact time: 30 min; adsorbent dosage: 1 g/L).

R^2 and RMSE parameters were used to determine the fit quality of isotherm models. Langmuir and Freundlich present R^2 close to 1 and smaller RMSE values, suggesting the suitability of both methods. As Langmuir model present the smallest RMSE values, it is considered the most suitable model to describe As(V) adsorption. However, as R^2 and RMSE values of Langmuir and Freundlich models are similar, arsenic adsorption can be described as a combination of electrostatic interactions and chemisorption – as demonstrated by the results of adsorption kinetics. Based on Langmuir results, the maximum adsorption capacities (Q_{max}) achieved were 32.8, 37.3, and 35.8 mg/g for $Y_2(CO_3)_3$), ZnO/TiO_2, and Fe_3O_4, respectively.

Langmuir isotherm assumes that adsorption occurs on a homogeneous surface and that all binding sites have an equal affinity for adsorbate, leading to the formation of an arsenic monolayer on the surface of the active material. Thus, this model considers adsorption as a chemisorption process [58]. On the other hand, Freundlich isotherm assumes that adsorption occurs on a heterogeneous surface and that the adsorption process is multilayer.

Many efforts have been devoted to the development of different adsorbents for arsenic removal from water. Previous works using similar adsorbents to those used in this work are presented in Table 1.

316 **Table 1.** Comparison of maximum adsorption capacities of different adsorbents for As removal from water.

Adsorbent	Adsorption capacity (mg/g)	Adsorbent dosage (g/L)	Initial concentration of As (mg/L)	Reference
Fe_3O_4 magnetite	0.147	10	1	[67]
α-Fe_2O_3	2.7	0.5	0.1 – 20	[65]
Hematite	14.46	1	1.5 – 12	[68]
Magnetite	**35.76**	**1**	**0.1 – 10**	**This study**
Fe_2O_3 – TiO_2	15.73	2	10 – 50	[69]
TiO_2 – ZrO_2	21.6	0.5	1	[70]
ZnO	0.85	2	0.2 – 2	[71]
ZnO/TiO_2	**37.30**	**1**	**0.1 – 10**	**This study**
Yttrium	35.56	4	1 – 60	[72]
$Y_2(CO_3)_3$	**32.83**	**1**	**0.1 – 10**	**This study**

317

318 Previous works using iron oxides for As adsorption present lower Q_{max} values when
319 compared with the Fe_3O_4 used in this work, using similar conditions [65, 67, 68]. The different
320 shapes of the magnetite used in this work and the higher PZC explain the highest Q_{max} values.
321 There is no previous report of the use of the ZnO/TiO_2 nanocomposite for As removal.
322 However, previous works using TiO_2 [69, 70] and ZnO [71] based nanocomposites for As(V)
323 removal present lower Q_{max} values. The superior surface area explains the higher Q_{max} values
324 achieved with this material compared with previous works. A previous work using yttrium-
325 based adsorbents presents a higher Q_{max} value than yttrium carbonate used in this work.
326 However, the experimental conditions used a higher adsorbent dosage (4 g/L) and contact time
327 (2 hours) when compared to this work (1 g/L and 30 minutes, respectively) [72]. Thus, the
328 sorbents used in this work achieved better or similar adsorption capacities when compared to
329 previous works using similar materials and experimental conditions, proving their affinity for
330 As(V) species adsorption. It is essential to notice that the adsorption capacity of the materials
331 used in this work was evaluated under arsenic concentrations and pH conditions similar to As-
332 contaminated water sources found worldwide, particularly in America [73], Europe [74], and
333 Asia [75].

334

335 **3.3. Adsorption mechanism**

FTIR spectroscopy was accessed to elucidate the adsorption mechanism of As(V) by the active materials. Figure 5 presents the FTIR spectra of all active materials before and after the As(V) adsorption experiments.

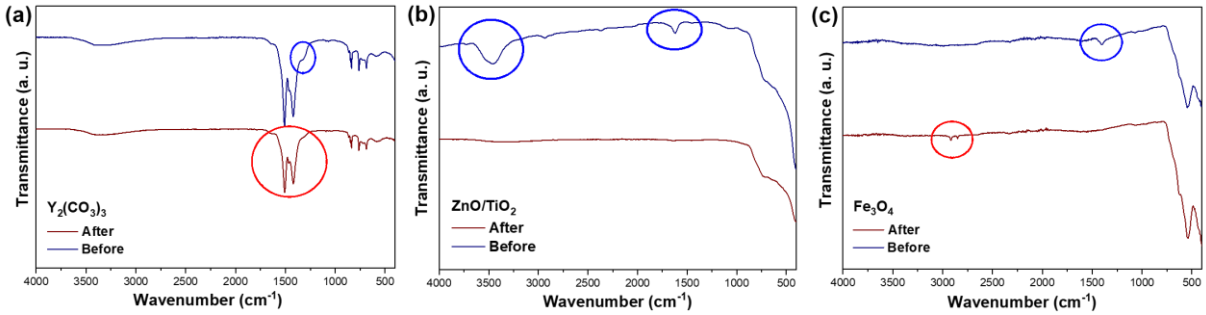

Figure 5. FTIR spectra of **(a)** $Y_2(CO_3)_3$, **(b)** ZnO/TiO_2, and **(c)** Fe_3O_4 before and after As(V) adsorption experiments.

FTIR spectra of $Y_2(CO_3)_3$ (Figure 5 a) shows a slight difference before and after adsorption of arsenic, decreasing peaks intensity at ≈ 1500 cm^{-1}. This group of peaks is associated with the carbonate groups of $Y_2(CO_3)_3$, which suggest the adsorption of As(V) on active material via ligand/anion exchange between CO_3^- groups and As(V) oxyanions [76]. In addition, an increase of peaks intensity was observed between ≈ 700 and 850 cm^{-1}, related to monodentate inner-sphere complex Y–O–As bonding [77]. These changes indicated that CO_3^- groups of Y-based active material are involved on As(V) adsorption via H-bonds interaction, by a chemisorption process, as described in equation 3 [29]:

$$\equiv Y - CO_3^{2-} + As\ (V)\ \rightarrow\ Y - As\ (V) + \ CO_3^{2-} \qquad (3)$$

$$\equiv Ti - OH + As\ (V)\ +\ H^+\ \rightarrow\ Ti - As\ (V) + \ H_2O \qquad (4)$$

$$\equiv Fe - OH + As\ (V)\ +\ H^+\ \rightarrow\ Fe - As\ (V) + \ H_2O \qquad (5)$$

Comparing the FTIR spectra of ZnO/TiO_2, two significant differences are observed before and after As(V) adsorption (Figure 5 b). A significant peak intensity decreases at ≈ 1600 and

3400 cm^{-1} is associated with H–O–H bonds and O–H stretching vibration of TiO_2. This indicates that the hydroxyl groups of the active material and the As(V) oxyanions are linked by a monodentate and bidentate complex on the adsorbent surface (equation 4) [78, 79].

FTIR spectra of Fe_3O_4 (Figure 5 c) present a substantial increase of intensity at peaks below ≈ 850 cm^{-1}, related to the coordination of Fe–O–As stretching vibration (equation 5) [80]. Further, two minor variations were observed, a decrease of peak intensity was found at ≈ 1500 cm^{-1}, associated with the complexation of Fe–OH groups with As(V) species [81]. The intensity increase of two peaks at ≈ 2950 cm^{-1} was related to As–O bonds between OH^- groups of Fe-based active material and arsenic oxyanions [82]. With this information, a complete understanding of the adsorption mechanism for all the active materials was established.

3.4. Acute lethality tests

To evaluate the putative toxic effects of Fe_3O_4, ZnO/TiO_2 and $Y_2(CO_3)_3$ nanoparticles, *D. magna* was exposed to water suspensions of these nanomaterials for 48 h. The pictures obtained after this exposure period are shown in Figure 6.

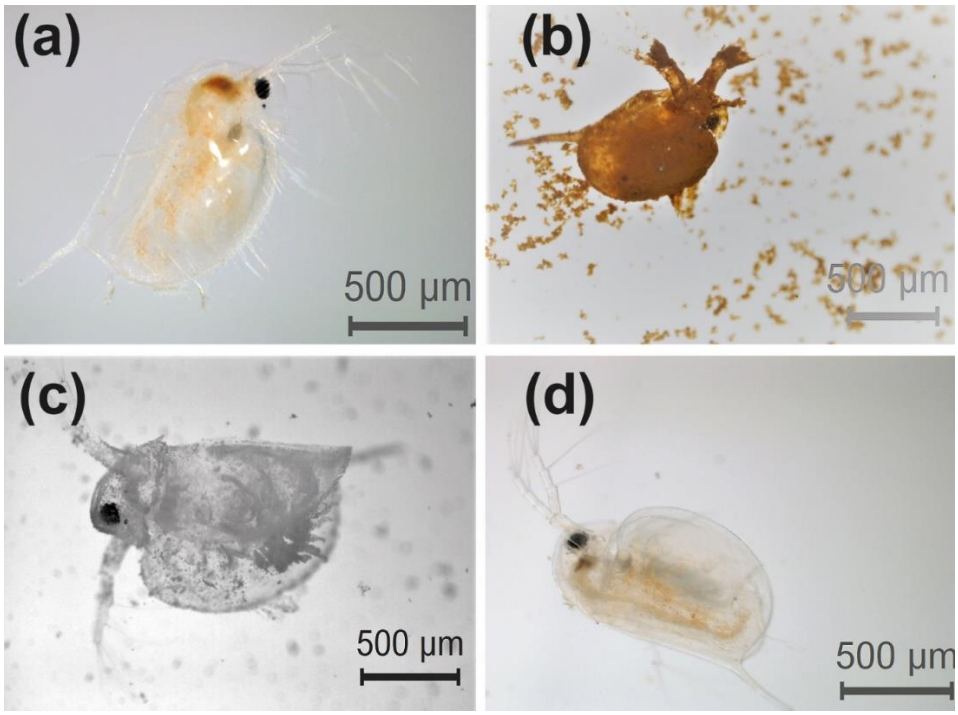

Figure 6. *Daphnia magna* exposed to **(a)** medium without nanoparticles and exposed to medium with nanoparticles: **(b)** Fe_3O_4, **(c)** ZnO/TiO_2, and **(d)** $Y_2(CO_3)_3$ after 48h.

Comparing Figure 6 (a) with Figure 6 (b – c), it is possible to realise that Fe_3O_4 and ZnO/TiO_2 nanoparticles uptake by *D. magna* occurred all over its body for both materials. Figure 6 (c) indicates that $Y_2(CO_3)_3$ nanoparticles accumulate mainly on the *D. magna* gut, which agrees with previous studies employing nanomaterials [76, 83].

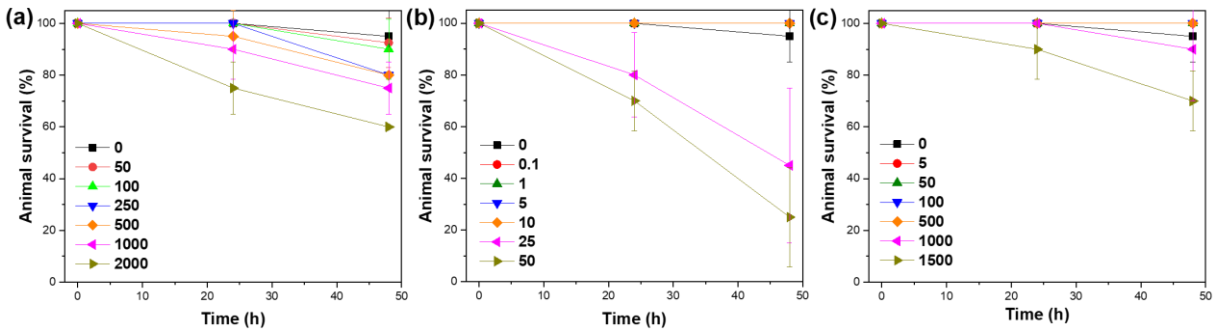

Figure 7. Acute lethal effects of **(a)** Fe_3O_4, **(b)** ZnO/TiO_2, and **(c)** $Y_2(CO_3)_3$ nanoparticles on *Daphnia magna* exposed to contaminated water for up to 48 hours (concentrations on mg/L).

Daphnia magna has been used as a model organism in ecotoxicity studies [84]. The present study shows that exposure to nanoparticles strongly affects *D. magna* survival, especially at the

highest tested concentrations of Fe_3O_4 (< 250 mg/L), ZnO/TiO_2 (< 25 mg/L) and $Y_2(CO_3)_3$ (1.5 mg/L) (Figure 7) (repeated-measurements ANOVA, $p < 0.05$). Mortality was higher for ZnO/TiO_2 (Figure 7 b) than for the remaining tested materials (Figure 7 a, c). However, mortality was low or absent at lower, environmentally relevant concentrations. The LC_{50} (95% C.I.) for Fe_3O_4, ZnO/TiO_2 and $Y_2(CO_3)_3$ was: $6.57x10^3$ mg/L ($2.73 – 20.31x10^3$ mg/L), 28.66 mg/L (21.12 – 32.66 mg/L), and $1.91x10^6$ mg/L ($1.63 – 3.09x10^6$ mg/L), respectively. Therefore, the toxicity tests show that the used micro/nanoparticles, besides their efficiency on As removal, do not threaten aquatic organisms, reinforcing their use for water treatments.

4. Conclusions

Three different active materials have been prepared and characterised, and their arsenic adsorption capacity evaluated. Magnetite nanoparticles show spherical and hexagonal shapes, with sizes ranging from 80 to 150 nm and a point of zero charges of ≈ 10. The prepared ZnO/TiO_2 nanoparticles are round-shaped with widths from 100 to 350 nm. A surface area of 88.28 m^2/g and a PZC of 6 characterises the nanocomposite. Yttrium carbonate exhibits shapes like nanorods with lengths ranging from 50 to 200 nm, and a PZC of 10. The pH proved to be an important parameter determining the adsorption capacity, and just the ZnO/TiO_2 nanocomposite presents high adsorption capacity for all the pH ranges. Contact time tests allow concluding that both yttrium and ZnO/TiO_2 present higher adsorption rates, achieving efficiencies close to 100% after 10 minutes of contact. Changing the initial concentration of As solution, ZnO/TiO_2 shows high performance on adsorption, with adsorption efficiencies always close to 100% in all ranges of concentrations (0.1 – 10 mg/L) and leading to maximum adsorption capacities of 32.83, 37.30, and 35.76 mg/g for $Y_2(CO_3)_3$, ZnO/TiO_2, and Fe_3O_4, respectively. In addition, toxicity tests using the model species *D. magna* showed that the micro/nanoparticles do not constitute a threat to aquatic organisms, reinforcing their use for

water remediation applications. The remarkable adsorption results indicate the suitability of all active materials for arsenic removal from contaminated water.

Credit author statement

Conceptualization: S. Lanceros-Mendez and P. M. Martins; Data curation: P. M. Martins; H. Salazar, Daniela Batista, Krishnapriya R.; Formal analysis: P. M. Martins, S. Lanceros-Mendez; Funding acquisition: S. Lanceros-Mendez and Fernanda Cássio; Investigation: H. Salazar, Daniela Batista, A. Fidalgo-Marijuan, Krishnapriya R., K. P. Shejale; Methodology: P. M. Martins, H. Salazar, K. P. Shejale , A. Fidalgo-Marijuan; Project administration: S. Lanceros-Mendez; Resources: S. Lanceros-Mendez, Fernanda Cássio, R. K. Sharma and G. Botelho; Software: H. Salazar, A. Fidalgo-Marijuan; Supervision: S. Lanceros-Mendez, Fernanda Cássio, R. K. Sharma, S. Ferdov and G. Botelho; Validation: S. Lanceros-Mendez, Fernanda Cássio and G. Botelho; Visualization: P. M. Martins; H. Salazar; Roles/Writing: H. Salazar and Daniela Batista; Writing - review & editing: P. M. Martins; S. Lanceros-Mendez, G. Botelho, S. Ferdov, and R. K. Sharma.

Acknowledgements

This work was supported by the Portuguese Foundation for Science and Technology (FCT) in the framework of the Strategic Projects UID/FIS/04650/2021 and UID/QUI/50006/2021 and project PTDC/FIS-MAC/28157/2017 and PTDC/BIA-BMA/30922/2017. H. Salazar and P. M. Martins thanks the FCT for grant SFRH/BD/122373/2016 and contract 2020.02802.CEECIND. The authors want to thank Águas do Norte, S. A., for the technical support provided in this work. Financial support from the Basque Government Industry Departments under the ELKARTEK programs is also acknowledged.

References

1. Montgomery, M.A. and M. Elimelech, *Water and sanitation in developing countries: Including health in the equation - Millions suffer from preventable illnesses and die every year.* Environmental Science and Technology, 2007. **41**(1): p. 17-24.
2. Han, Y., et al., *Preparation of Cu-Y binary oxysulfide and its application in the removal of arsenic from aqueous solutions.* Separation and Purification Technology, 2019: p. 410-418.
3. Mandal, B.K. and K.T. Suzuki, *Arsenic round the world: A review.* Talanta, 2002. **58**(1): p. 201-235.
4. Alam, R. and K. McPhedran, *Applications of biological sulfate reduction for remediation of arsenic – A review.* Chemosphere, 2019. **222**: p. 932-944.
5. Srivastava, P.K., et al., *Biological removal of arsenic pollution by soil fungi.* Science of the Total Environment, 2011. **409**(12): p. 2430-2442.
6. Basu, A., et al., *A review on sources, toxicity and remediation technologies for removing arsenic from drinking water.* Research on Chemical Intermediates, 2014. **40**(2): p. 447-485.
7. Van Halem, D., et al., *Arsenic in drinking water: A worldwide water quality concern for water supply companies.* Drinking Water Engineering and Science, 2009. **2**(1): p. 29-34.
8. Kowalski, K.P., *Chapter 8 - Advanced Arsenic Removal Technologies Review A2 - Søgaard, Erik G*, in *Chemistry of Advanced Environmental Purification Processes of Water*. 2014, Elsevier: Amsterdam. p. 285-337.
9. Shannon, M.A., et al., *Science and technology for water purification in the coming decades.* Nature, 2008. **452**(7185): p. 301-310.
10. Salazar, H., et al., *Poly(vinylidene fluoride-hexafluoropropylene)/bayerite composite membranes for efficient arsenic removal from water.* Materials Chemistry and Physics, 2016. **183**: p. 430-438.
11. Wei, Y., et al., *Fast and efficient removal of As(III) from water by CuFe2O4 with peroxymonosulfate: Effects of oxidation and adsorption.* Water Research, 2019: p. 182-190.
12. Eslami, H., et al., *Enhanced coagulation process by Fe-Mn bimetal nano-oxides in combination with inorganic polymer coagulants for improving As(V) removal from contaminated water.* Journal of Cleaner Production, 2019. **208**: p. 384-392.
13. Alguacil, F.J. and E. Escudero, *Removal of arsenic(V) from aqueous wastes by ion exchange with lewatit MP64 resin.* Desalination and Water Treatment, 2018. **133**: p. 257-261.
14. Yue, T., et al., *Arsenic(V) adsorption on ferric oxyhydroxide gel at high alkalinity for securely recycling of arsenic-bearing copper slag.* Applied Surface Science, 2019. **478**: p. 213-220.
15. Wang, J., et al., *Multi-functionalization of magnetic graphene by surface-initiated ICAR ATRP mediated by polydopamine chemistry for adsorption and speciation of arsenic.* Applied Surface Science, 2019. **478**: p. 15-25.
16. Asere, T.G., C.V. Stevens, and G. Du Laing, *Use of (modified) natural adsorbents for arsenic remediation: A review.* Science of the Total Environment, 2019. **676**: p. 706-720.
17. Nieto-Delgado, C., J. Gutiérrez-Martínez, and J.R. Rangel-Méndez, *Modified activated carbon with interconnected fibrils of iron-oxyhydroxides using Mn2 + as morphology regulator, for a superior arsenic removal from water.* Journal of Environmental Sciences (China), 2019. **76**: p. 403-414.
18. Majumder, C., *Arsenic(V) Removal Using Activated Alumina: Kinetics and Modeling by Response Surface.* Journal of Environmental Engineering (United States), 2018. **144**(3).
19. Shadbahr, J. and T. Husain, *Affordable and efficient adsorbent for arsenic removal from rural water supply systems in Newfoundland.* Science of the Total Environment, 2019. **660**: p. 158-168.
20. Yenial, Ü. and G. Bulut. *Single and binary adsorption of arsenic and lead onto red mud and coal waste*. in *IMPC 2018 - 29th International Mineral Processing Congress*. 2019.
21. Khosa, M.A., J. Wu, and A. Ullah, *Chemical modification, characterization, and application of chicken feathers as novel biosorbents.* RSC Advances, 2013. **3**(43): p. 20800-20810.

22. Amer, M.W. and A.M. Awwad, *Removal of As(V) from aqueous solution by adsorption onto nanocrystalline kaolinite: Equilibrium and thermodynamic aspects of adsorption.* Environmental Nanotechnology, Monitoring and Management, 2018. **9**: p. 37-41.
23. Jacobson, A.T. and M. Fan, *Evaluation of natural goethite on the removal of arsenate and selenite from water.* Journal of Environmental Sciences (China), 2019. **76**: p. 133-141.
24. Pincus, L.N., et al., *Multifunctional photoactive and selective adsorbent for arsenite and arsenate: Evaluation of nano titanium dioxide-enabled chitosan cross-linked with copper.* Journal of Hazardous Materials, 2018. **358**: p. 145-154.
25. He, Z., S. Tian, and P. Ning, *Adsorption of arsenate and arsenite from aqueous solutions by cerium-loaded cation exchange resin.* Journal of Rare Earths, 2012. **30**(6): p. 563-572.
26. Maziarz, P., et al., *Highly effective magnet-responsive LDH-Fe oxide composite adsorbents for As(V) removal.* Chemical Engineering Journal, 2019. **362**: p. 207-216.
27. Ghosh, S., R. Prabhakar, and S.R. Samadder, *Performance of γ-aluminium oxide nanoparticles for arsenic removal from groundwater.* Clean Technologies and Environmental Policy, 2019. **21**(1): p. 121-138.
28. Khwamsawat, K., J. Mahujchariyawong, and S. Danwittayakul, *Using ZnO nanorods coated porous ceramic monolith to remove arsenic from groundwater*, in *Key Engineering Materials*. 2017. p. 756-765.
29. Chen, C., et al., *Mechanism of Arsenate Adsorption by Basic Yttrium Carbonate in a Fixed-Bed Column.* Environmental Engineering Science, 2017. **34**(11): p. 785-791.
30. Velazquez-Peña, G.C., et al., *As(V) sorption by different natural zeolite frameworks modified with Fe, Zr and FeZr.* Microporous and Mesoporous Materials, 2019. **273**: p. 133-141.
31. Baskan, M.B. and A. Pala, *Batch and fixed-bed column studies of arsenic adsorption on the natural and modified clinoptilolite.* Water, Air, and Soil Pollution, 2014. **225**(1).
32. Zhang, W., et al., *Enhanced removal of arsenite and arsenate by a multifunctional Fe-Ti-Mn composite oxide: Photooxidation, oxidation and adsorption.* Water Research, 2018. **147**: p. 264-275.
33. Yu, Y., et al., *Yttrium-doped iron oxide magnetic adsorbent for enhancement in arsenic removal and ease in separation after applications.* Journal of Colloid and Interface Science, 2018. **521**: p. 252-260.
34. Guan, X., et al., *Application of titanium dioxide in arsenic removal from water: A review.* Journal of Hazardous Materials, 2012. **215-216**: p. 1-16.
35. Joshi, S., et al., *Arsenic Removal from Water by Adsorption onto Iron Oxide/Nano-Porous Carbon Magnetic Composite.* Applied Sciences, 2019. **9**(18): p. 3732.
36. Shejale, K.P., et al., *Zinc Oxide–Titania Heterojunction-based Solid Nanospheres as Photoanodes for Electron-Trapping in Dye-Sensitized Solar Cells.* Energy Technology, 2017. **5**(3): p. 489-494.
37. Singh, P., et al., *Kinetics and mechanism of arsenic removal using sulfide-modified nanoscale zerovalent iron.* Chemical Engineering Journal, 2021. **412**.
38. Bullen, J.C., et al., *A Revised Pseudo-Second-Order Kinetic Model for Adsorption, Sensitive to Changes in Adsorbate and Adsorbent Concentrations.* Langmuir, 2021. **37**(10): p. 3189-3201.
39. Syafiuddin, A., et al., *Application of the kinetic and isotherm models for better understanding of the behaviors of silver nanoparticles adsorption onto different adsorbents.* Journal of Environmental Management, 2018. **218**: p. 59-70.
40. Sawood, G.M. and S.K. Gupta, *Kinetic equilibrium and thermodynamic analyses of As (V) removal from aqueous solution using iron-impregnated Azadirachta indica carbon.* Applied Water Science, 2020. **10**(6): p. 131.
41. Ahmed, W., et al., *Adsorption of arsenic (III) from aqueous solution by a novel phosphorus-modified biochar obtained from Taraxacum mongolicum Hand-Mazz: Adsorption behavior and mechanistic analysis.* Journal of Environmental Management, 2021. **292**.

42. Huo, J.B. and G. Yu, *Mesoporous cerium oxide-anchored magnetic polyhedrons derived from MIL-100(Fe) for enhanced removal of arsenite from aqueous solution.* Journal of Hazardous Materials, 2021. **415**.
43. Zoroufchi Benis, K., et al., *Enhanced arsenate removal by Fe-impregnated canola straw: assessment of XANES solid-phase speciation, impacts of solution properties, sorption mechanisms, and evolutionary polynomial regression (EPR) models.* Environmental Science and Pollution Research, 2021. **28**(10): p. 12659-12676.
44. Muedi, K.L., et al., *Effective removal of arsenate from wastewater using aluminium enriched ferric oxide-hydroxide recovered from authentic acid mine drainage.* Journal of Hazardous Materials, 2021. **414**.
45. Sakuma, M., *Probit analysis of preference data.* Applied Entomology and Zoology, 1998. **33**: p. 339-347.
46. Zar, J.H., *Biostatistical Analysis (5th Edition)*. 2007: Prentice-Hall, Inc.
47. Devi, H.F. and T.D. Singh, *Optical properties of porous Sm3+-doped yttrium orthophosphate nanoparticles tailored by co-precipitation route.* Optics Communications, 2019. **439**: p. 34-37.
48. Gao, S., et al., *Effect of different Co contents on the microstructure and tensile strength of Mg-Co-Y alloys.* Materials Science and Engineering: A, 2019. **750**: p. 91-97.
49. Zhang, Y., et al., *Improved hydrogen storage performances of Mg-Y-Ni-Cu alloys by melt spinning.* Renewable Energy, 2019: p. 263-271.
50. Balbuena, J., et al., *Hematite porous architectures as enhanced air purification photocatalyst.* Journal of Alloys and Compounds, 2019. **797**: p. 166-173.
51. Jayashree, M., M. Parthibavarman, and S. Prabhakaran, *Hydrothermal-induced a-Fe2O3/graphene nanocomposite with ultrahigh capacitance for stabilized and enhanced supercapacitor electrodes.* Ionics, 2019. **25**(7): p. 3309-3319.
52. Nur, T., et al., *Removing arsenic from water by coprecipitation with iron: Effect of arsenic and iron concentrations and adsorbent incorporation.* Chemosphere, 2019. **226**: p. 431-438.
53. Teixeira, S., et al., *Reusability of photocatalytic TiO2 and ZnO nanoparticles immobilized in poly(vinylidene difluoride)-co-trifluoroethylene.* Applied Surface Science, 2016. **384**: p. 497-504.
54. Ahmed, M.A., et al., *Control synthesis of metallic gold nanoparticles homogeneously distributed on hexagonal ZnO nanoparticles for photocatalytic degradation of methylene blue dye.* Environmental Nanotechnology, Monitoring and Management, 2019. **12**.
55. Hashemzadeh, M., A. Nilchi, and A.H. Hassani, *Synthesis of novel surface-modified hematite nanoparticles for lead ions removal from aqueous solution.* Materials Chemistry and Physics, 2019. **227**: p. 279-290.
56. Yapryntsev, A.D., et al., *Exfoliation of layered yttrium hydroxide by rapid expansion of supercritical suspensions.* Journal of Supercritical Fluids, 2019: p. 40-48.
57. Lee, S.H., et al., *Enhanced arsenate removal performance in aqueous solution by yttrium-based adsorbents.* International Journal of Environmental Research and Public Health, 2015. **12**(10): p. 13523-13541.
58. Sherlala, A.I.A., et al., *Adsorption of arsenic using chitosan magnetic graphene oxide nanocomposite.* Journal of Environmental Management, 2019. **246**: p. 547-556.
59. Altowayti, W.A.H., et al., *The adsorptive removal of As (III) using biomass of arsenic resistant Bacillus thuringiensis strain WS3: Characteristics and modelling studies.* Ecotoxicology and Environmental Safety, 2019. **172**: p. 176-185.
60. Yin, Y., et al., *Adsorption of arsenic by activated charcoal coated zirconium-manganese nanocomposite: Performance and mechanism.* Colloids and Surfaces A: Physicochemical and Engineering Aspects, 2019. **575**: p. 318-328.
61. Sherlala, A.I.A., A.A.A. Raman, and M.M. Bello, *Synthesis and characterization of magnetic graphene oxide for arsenic removal from aqueous solution.* Environmental Technology (United Kingdom), 2019. **40**(12): p. 1508-1516.

62. Uppal, H., et al., *Zinc peroxide functionalized synthetic graphite: An economical and efficient adsorbent for adsorption of arsenic (III) and (V).* Journal of Environmental Chemical Engineering, 2016. **4**(3): p. 2964-2975.
63. Vivek Vardhan, C.M. and M. Srimurali, *Defluoridation of drinking water using a novel sorbent: lanthanum-impregnated green sand.* Desalination and Water Treatment, 2016. **57**(1): p. 202-212.
64. Zhang, W., et al., *Efficient oxidation and sorption of arsenite using a novel titanium(IV)-manganese(IV) binary oxide sorbent.* Journal of Hazardous Materials, 2018. **353**: p. 410-420.
65. Majumder, A., et al., *Green synthesis of iron oxide nanoparticles for arsenic remediation in water and sludge utilization.* Clean Technologies and Environmental Policy, 2019. **21**(4): p. 795-813.
66. Vivona, R., et al., *Occurrence of minor toxic elements in volcanic-sedimentary aquifers: a case study in central Italy.* Hydrogeology Journal, 2007. **15**(6): p. 1183-1196.
67. Kanel, S.R. and H. Choi, *Removal of arsenic from groundwater by industrial byproducts and its comparison with zero-valent iron.* Journal of Hazardous, Toxic, and Radioactive Waste, 2017. **21**(3).
68. Yang, X., et al., *Adsorption of As(III) on porous hematite synthesized from goethite concentrate.* Chemosphere, 2017. **169**: p. 188-193.
69. Su, H., et al., *Arsenic removal from water by photocatalytic functional Fe2O3–TiO2 porous ceramic.* Journal of Porous Materials, 2017. **24**(5): p. 1227-1235.
70. Khayyun, T.S. and A.H. Mseer, *Comparison of the experimental results with the Langmuir and Freundlich models for copper removal on limestone adsorbent.* Applied Water Science, 2019. **9**(8): p. 170.
71. Muensri, P. and S. Danwittayakul, *Removal of arsenic from groundwater using nano-metal oxide adsorbents*, in *Key Engineering Materials*. 2017. p. 766-772.
72. Yu, Y., et al., *An innovative yttrium nanoparticles/PVA modified PSF membrane aiming at decontamination of arsenate.* Journal of Colloid and Interface Science, 2018. **530**: p. 658-666.
73. Dummer, T.J., et al., *Geostatistical modelling of arsenic in drinking water wells and related toenail arsenic concentrations across Nova Scotia, Canada.* Sci Total Environ, 2015. **505**: p. 1248-58.
74. Komorowicz, I. and D. Barałkiewicz, *Determination of total arsenic and arsenic species in drinking water, surface water, wastewater, and snow from Wielkopolska, Kujawy-Pomerania, and Lower Silesia provinces, Poland.* Environ Monit Assess, 2016. **188**(9): p. 504.
75. Sarkar, A. and B. Paul, *The global menace of arsenic and its conventional remediation - A critical review.* Chemosphere, 2016. **158**: p. 37-49.
76. Chen, C., et al., *Efficient degradation of roxarsone and simultaneous in-situ adsorption of secondary inorganic arsenic by a combination of Co3O4-Y2O3 and peroxymonosulfate.* Journal of Hazardous Materials, 2021. **407**: p. 124559.
77. He, J., et al., *New insight into adsorption and co-adsorption of arsenic and tetracycline using a Y-immobilized graphene oxide-alginate hydrogel: Adsorption behaviours and mechanisms.* Science of The Total Environment, 2020. **701**: p. 134363.
78. Li, Y., et al., *UV-induced photoactive adsorption mechanism of arsenite by anatase TiO2 with high surface hydroxyl group density.* Colloids and Surfaces A: Physicochemical and Engineering Aspects, 2014. **462**: p. 202-210.
79. Dou, X., et al., *Arsenate adsorption on an Fe–Ce bimetal oxide adsorbent: EXAFS study and surface complexation modeling.* Colloids and Surfaces A: Physicochemical and Engineering Aspects, 2011. **379**(1): p. 109-115.
80. Huo, L., et al., *Enhanced removal of As (V) from aqueous solution using modified hydrous ferric oxide nanoparticles.* Scientific Reports, 2017. **7**(1): p. 40765.
81. Devi, R.R., et al., *Removal of iron and arsenic (III) from drinking water using iron oxide-coated sand and limestone.* Applied Water Science, 2014. **4**(2): p. 175-182.

82. Karimi, P., et al., *Arsenic Removal from Mining Effluents Using Plant-Mediated, Green-Synthesized Iron Nanoparticles.* Processes, 2019. **7**(10).
83. Yan, N. and W.-X. Wang, *Novel Imaging of Silver Nanoparticle Uptake by a Unicellular Alga and Trophic Transfer to Daphnia magna.* Environmental Science & Technology, 2021. **55**(8): p. 5143-5151.
84. Altshuler, I., et al., *An integrated multi-disciplinary approach for studying multiple stressors in freshwater ecosystems: Daphnia as a model organism.* Integr Comp Biol, 2011. **51**(4): p. 623-33.

Supplementary Information

1. Supplementary information for sub-chapter 2.3.

The kinetic curves were fitted according to nonlinear forms of pseudo-first, pseudo-second-order, Elovich, and Bangham models described in equations 1, 2, 3, and 4, respectively:

$$\mathrm{Q_t} = Q_e\left(1 - exp^{(-k_1 t)}\right) \quad (1)$$

$$\mathrm{Q_t} = \frac{Q_e^2 k_2 t}{1+Q_e K_2 t} \quad (2)$$

$$Q_t = \frac{\ln \alpha\beta}{\beta} + \frac{1}{\beta}\ln t \qquad (3)$$

$$Q_t = kt^{\upsilon} \qquad (4)$$

where Q_e and Q_t (mg/g) are the capacities for arsenic adsorption at equilibrium and at a correspondent time, respectively. K_1 (min^{-1}) is the pseudo-first-order adsorption rate constant, K_2 (g/mg min) is the pseudo-second-order adsorption rate constant, α is the initial adsorption rate (mg/g min), and β is the desorption constant (g/mg), k (mg/g) and υ (min^{-1}) are constants.

The isotherm curves were fitted to the following models: Langmuir, Freundlich, Temkin, and Dubinin-Radushkevich, which are defined by the equations 5 to 9, respectively:

$$q_e = \frac{Q_{max} b C_e}{1 + bC_e} \qquad (5)$$

$$q_e = K_F C_e^{1/n} \qquad (6)$$

$$q_e = \frac{RT}{b_T}\ln(K_T C_e) \qquad (7)$$

$$q_e = Q_S exp^{(-B_D \varepsilon^2)} \qquad (8)$$

$$\varepsilon = RT \ln\left(1 + \frac{1}{C_e}\right) \qquad (9)$$

where q_e (mg/g) is the As adsorption capacity at a given equilibrium concentration, C_e (mg/L) is the arsenic equilibrium concentration, q_{max} (mg/g) is the maximum adsorption capacity, K_L (L/mg) is the adsorption rate for Langmuir isotherm model, K_F ($L^{1/n}$ $mg^{(1-1/n)}$ g^{-1}) is the adsorption capacity of the adsorbent for Freundlich isotherm model, and *1/n* is a measure of the adsorption intensity, b (J/mol) is Temkin constant, K_T (L/g) Temkin isotherm constant, Q_S (mg/g) is the maximum adsorption capacity, B_D (mol^2/kJ^2) is Dubinin-Radushkevich constant, ε (kJ/mol) is the adsorption potential, R (8.314 J/mol K) is the universal gas constant, T (K) is the temperature, k and υ are constants. Regarding *1/n* value, the closer its value to 0, the more heterogeneous is the surface of the nanocomposite membrane.

2. Supplementary information for sub-chapter 2.4.

Table S2. pH of the nanosuspensions measured at the beginning and after 48h of exposure.

Treatments	Concentrations (mg/L)	pH	
		Initial	48 h
Control	0	8.29	8.07
Fe_3O_4	50	8.20	7.81
	100	8.11	7.80
	250	7.77	7.84
	500	7.45	7.99
	1000	7.18	7.64
	2000	6.78	7.49
ZnO/TiO_2	0.1	8.09	7.63
	1	8.12	7.71
	5	8.12	7.69
	10	8.09	7.74
	25	8.03	7.84
	50	7.93	7.96
$Y_2(CO_3)_3$	0.005	8.02	7.74
	0.05	8.10	7.79
	0.1	8.11	7.77
	0.5	8.12	7.83
	1	8.11	7.86
	1.5	8.10	7.88

3. Supplementary information for sub-chapter 3.2.2.

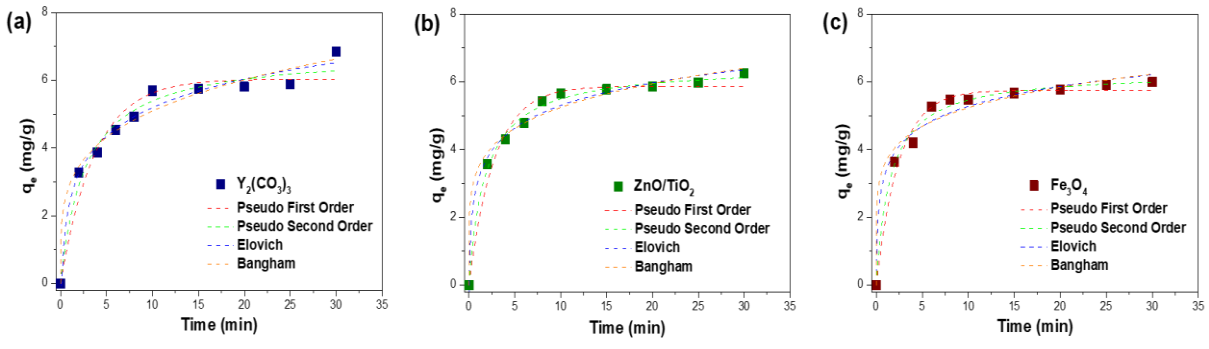

Figure S8. Adsorption kinetics of **(a)** $Y_2(CO_3)_3$, **(b)** ZnO/TiO_2, and **(c)** Fe_3O_4, for As (V) removal ([As] = 100 µg/L; contact time: 30 min; pH = 7).

Table S3. Pseudo-first-order, pseudo-second-order, Elovich, and Bangham kinetics models for As(V) adsorption by $Y_2(CO_3)_3$, ZnO/TiO_2, and Fe_3O_4 active materials.

	Parameter	$Y_2(CO_3)_3$	ZnO/TiO_2	Fe_3O_4
Pseudo First Order	**k_1 (min^{-1})**	0.269	0.361	0.407
	R^2	0.95	0.98	0.98
	RMSE	0.459	0.307	0.257
Pseudo Second Order	**k_2 (g/mg min)**	0.054	0.085	0.104
	R^2	0.97	0.994	0.991
	RMSE	0.292	0.123	0.158
Elovich	**α (mg/g min)**	8.831	23.908	42.488
	R^2	0.97	0.98	0.97
	RMSE	0.301	0.222	0.276
Bangham	**k (mg/g)**	0.240	3.457	3.632
	R^2	0.97	0.98	0.97
	RMSE	0.312	0.271	0.317

4. Supplementary information for sub-chapter 3.2.3.

Table S4. Effect of As (V) concentration on efficiency (E) and adsorption capacity (Q_e) of active materials.

[As] (mg/L)	$Y_2(CO_3)_3$		ZnO/TiO_2		Fe_3O_4	
	E (%)	**Q_e (mg/g)**	**E (%)**	**Q_e (mg/g)**	**E (%)**	**Q_e (mg/g)**
0.1	99.6	0.10	99.9	0.10	99.8	0.10
0.25	98.9	0.25	98.7	0.25	98.1	0.25
0.5	98.7	0.49	99.4	0.50	98.9	0.49
0.75	98.9	0.74	99.3	0.74	98.5	0.74
1	98.9	0.99	99.4	0.99	98.8	0.99

2	97.9	1.96	98.6	1.97	98.1	1.96
5	97.5	4.88	98.0	4.90	97.9	4.89
10	97.2	9.72	97.9	9.79	97.6	9.76

748

749

750 **Table S5.** Isotherm models parameters for As (V) removal by $Y_2(CO_3)_3$), ZnO/TiO_2, and Fe_3O_4.

Model	Parameter	$Y_2(CO_3)_3$	ZnO/TiO_2	Fe_3O_4
Langmuir	**Q_{max} (mg/g)**	32.83	37.30	35.76
	K_L (L/mg)	1.49	1.67	1.54
	R^2	0.994	0.99	0.997
	RMSE	0.149	0.328	0.133
Freundlich	**K_F ($mg^{n-1} L^n/g$)**	26.83	33.25	31.93
	1/n	0.80	0.79	0.84
	R^2	0.998	0.994	0.998
	RMSE	0.169	0.286	0.160
Temkin	**b_T (J/mol)**	1.35	1.16	1.23
	K_T (L/g)	436.49	943.92	539.42
	R^2	0.7	0.6	0.6
	RMSE	1.720	1.863	1.938
Dubinin – Radushkevich	**Q_S (mg/g)**	15.38	16.52	16.14
	B_D (mol^2/kJ^2)	0.21	0.18	0.20
	R^2	0.97	0.97	0.98
	RMSE	0.528	0.616	0.440

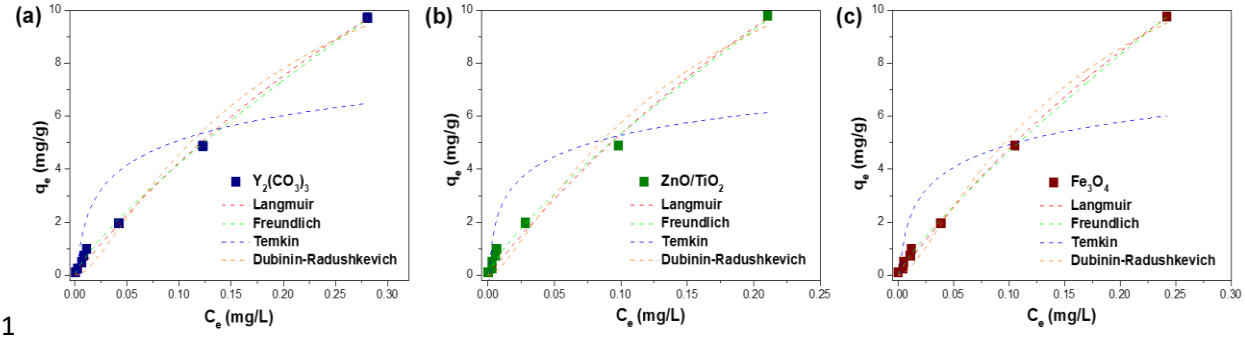

751

752 **Figure S9.** Adsorption isotherm models simulation for **(a)** $Y_2(CO_3)_3$, **(b)** ZnO/TiO_2, and **(c)** Fe_3O_4, for As (V)
753 removal (contact time: 30 min; pH = 7).

754